Russian Geology and Geophysics © 2020, V.S. Sobolev IGM, Siberian Branch of the RAS
Vol. 61, No. 9, pp. 937–950, 2020 *DOI:10.15372/RGG2020161* *Geologiya i Geofizika*

Chlorine in the Earth's Mantle as an Indicator of the Global Recycling of Oceanic Crust

E.V. Asafov[a, ✉], A.V. Sobolev[a,b], V.G. Batanova[a,b], M.V. Portnyagin[a,c]

[a] *Vernadsky Institute of Geochemistry and Analytical Chemistry, Russian Academy of Sciences, ul. Kosygina 19, Moscow, 119991, Russia*

[b] *Université Grenoble Alpes, Institut des Sciences de la Terre (ISTerre), CNRS, F-38041, Grenoble, France*

[c] *GEOMAR Helmholtz Centre for Ocean Research Kiel, Wischhofstrasse 1-3, 24148, Kiel, Germany*

Received 15 May 2020; accepted 29 June 2020

Abstract— Homogenized melt inclusions in olivine were studied in Archean komatiites from the Barberton Greenstone Belt, Weltevreden Formation in South Africa (3.3 Ga), Abitibi Greenstone Belt in Canada (2.72 Ga), and the Belingwe Greenstone Belt in Zimbabwe (2.69 Ga). Contamination of the komatiite melts with crustal material enriched in Rb, Cl, and H_2O during the crystallization of olivine is demonstrated. Uncontaminated melts have mantle Rb/Nb ratios but are significantly enriched in Cl and H_2O relative to K and Ce, respectively, exhibiting similar incompatibility during crystallization and partial mantle melting. These observations suggest the presence of a chlorine- and water-enriched mantle source before 3.3 Ga. The excess Cl and H_2O contents in the komatiites are assumed to result from the interaction of partially molten mantle plumes with the mantle transition zone. The most likely source of Cl and H_2O enriching the deep mantle is the oceanic lithosphere that endured a seafloor alteration. We conclude that the recycling of the altered oceanic lithosphere into the mantle, probably via subduction, began in the first billion years of the Earth's history. Delamination of the Archean crust could not cause transport of chlorine and water into the deep mantle.

Keywords: melt inclusions; komatiites; mantle petrology; transition zone; water in mantle; geochemistry of volatiles; plume magmatism; Archean mantle; plate tectonics

INTRODUCTION

Earth possesses unique, unknown for any other planets features, such as life, water in three states on its surface, and the regime of global plate tectonics. The plate tectonics controls the matter and energy exchange between the mantle and surface reservoirs and probably caused the first two features. The causes and time of the plate tectonics initiation remain open questions (Korenaga, 2008).

One possibility to solve this problem is to determine the start of global exchange between the interior of the planet and its surface, which can be done by tracing the temporal evolution of typical crustal element concentrations in the deep mantle. Komatiites – ultramafic magmas formed by high degree of mantle melting – are perspective for such study as they contain information the deep mantle composition since at least 3.6 Ga (Arndt et al., 2008; Herzberg, 2016). However, Archean rocks lack the information about the characteristic crustal components such as mobile elements (U, Pb, Rb, Sr) and volatiles (H, C, Cl) due to crustal contamination, degassing, and post-magmatic alteration. A possible solution of this problem is study of melt inclusions in minerals that are formed during crystallization of magma and protected from the external processes by their hosts (Sobolev, 1996). The perspectives of melt inclusion studies in komatiites have been demonstrated in a number of studies, which allowed to identify the significant excess of H_2O and deficiency of Pb in the deep mantle starting at least from 3.3 Ga (Kamenetsky et al., 2010; Gurenko et al., 2011, 2016; Sobolev et al., 2016, 2019; Asafov et al., 2018).

In this paper, we used the methods of melt inclusion studies to characterize the behavior of chlorine in the mantle sources and at crystallization of komatiites. The obtained results suggest a significant chlorine enrichment in the Earth's deep mantle and provide further evidence for the proposed start of the global recycling of the upper oceanic lithosphere in the Paleoarchean.

GEOLOGICAL BACKGROUND AND SAMPLES

Here we present the results obtained for komatiites from three different Archean greenstone belts (Fig. 1).

✉ Corresponding author.
E-mail address: evasafov@gmail.com (E.V. Asafov)

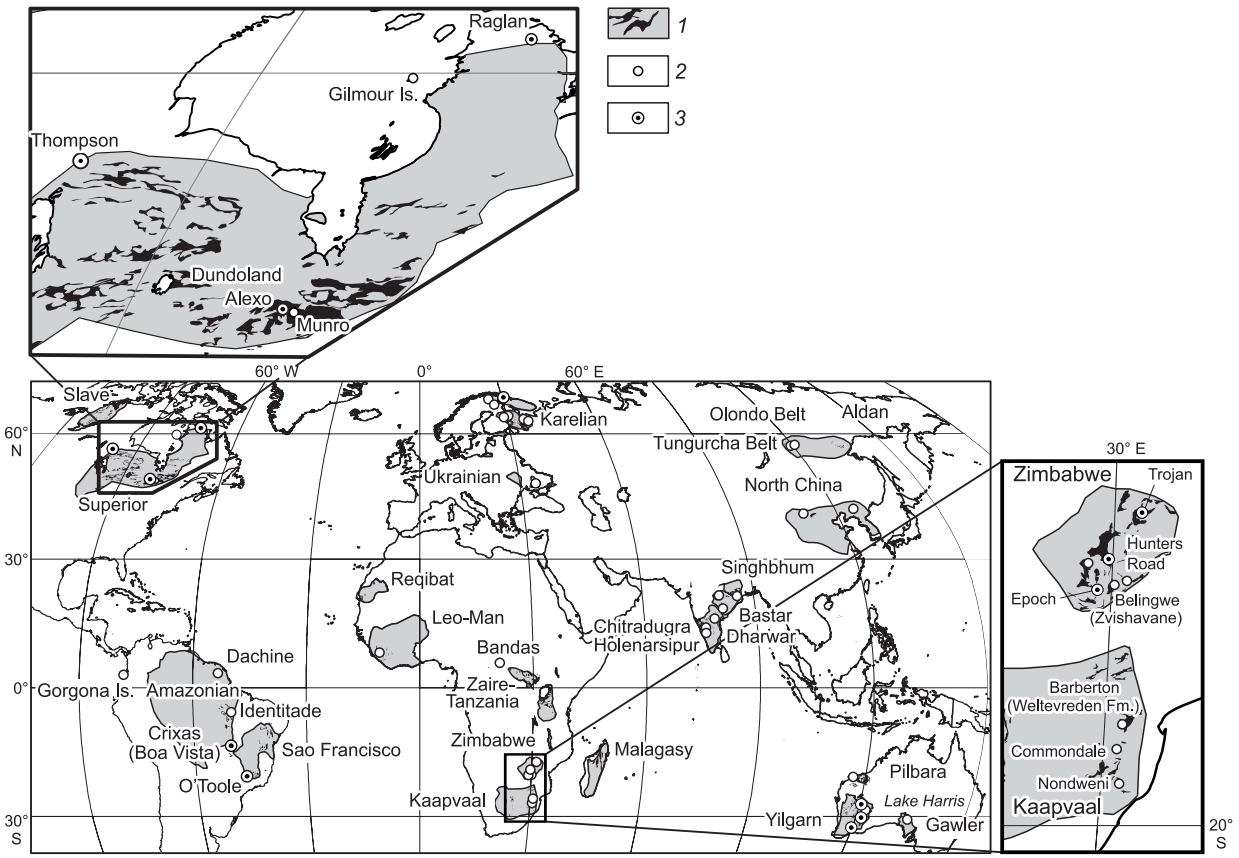

Fig. 1. World map showing major komatiite localities, modified after Arndt et al. (2008). Komatiites are present in almost all Archean cratons. Legend: *1*, Archean and Paleoproterozoic cratons (grey) and greenstone belts (black stripes); *2*, Komatiite localities; *3*, Komatiite localities associated with Ni-Fe-Cu-PGE sulfide ores.

Abitibi. Komatiites from the Abitibi Greenstone belt, Canada have an age of 2.72 ± 0.02 Ga (Pb-Pb method, (Brévart et al., 1986)). Three samples of olivine cumulates were collected during field works in the Munro Township area in 2014. Samples #805 and #810 are from the type locality Pyke Hill outcrop (Pyke et al., 1973). Sample 823 was collected from the Alexo flow, which belongs to the contemporaneous volcanic sequence. The Abitibi Greenstone Belt predominantly consists of volcanic rocks that comprise ultramafic, mafic and tholeiitic lavas. The detailed geological background of the Munro area has been reported in a number of papers (Pyke et al., 1973; Arndt et al., 1977; Muir and Comba, 1979).

The Abitibi komatiite flows were subjected to low grade metamorphism and partially or completely serpentinized, and did not preserve the initial magmatic characteristics. Nonetheless, the basal parts of these flows, namely the cumulate layers, contain fresh magmatic olivine hosting rare melt inlcusions.

Belingwe. The 2.69 ± 0.01 Ga Belingwe Greenstone Belt, Zimbabwe (Pb-Pb method, (Dupre and Arndt, 1990)) is located within the southern part of the Zimbabwe craton and consists of volcanigenic and sedimentary complexes. The detailed geological background of the Belingwe Greenstone Belt is discussed in a series of papers by Bickle et al. (1975, 1977, 1993) and Nisbet et al. (1977). In this study we examined olivine cumulate (sample #z6) hammered from the Tony's flow at the SASKMAR drill site. This flow belongs to the Reliance Formation, the upper greenstone complex of Belingwe (Bickle et al., 1993) and is one the most accessible and well preserved komatiite flows in the Belingwe Greenstone Belt. In contrast to many other komatiites as well as other Archean rocks, the Belingwe komatiites are uniquely fresh and contain abundant relicts of big and fresh magmatic olivine grains plunged into altered groundmass.

Barberton, Weltevreden. The 3.26–3.55 Ga Barberton Greenstone Belt, South Africa (Armstrong et al., 1990; Byerly et al., 1996; Kröner et al., 1996) is located in the northeastern part of the country within the ancient Kaapvaal Craton, which forms the core of the southern part of Africa. Barberton Greenstone Belt is one of the biggest among the five Kaapvaal craton Archean greenstone belts. It is 15 km thick and comprises three major groups – Onverwacht, Fig Tree and Moodies groups. The detailed geological background of this region is given in (Lowe and Byerly, 2007). A set of komatiite samples for this study was collected from the 3.27 ± ± 0.01 Ga (Re-Os, (Connolly et al., 2011)) Weltevreden formation in the northern part of the Barberton Greenstone Belt.

The Weltevreden Formation is related to the Onverwacht group and comprises komatiites, basalts, komatiitic tuffs and ultramafic intrusions with a total thickness of a few kilometers. Komatiite flows (10–500 m thick), sills and tuffs represent up to 80% of the formation. The exact structure and stratigraphy of the Weltevreden Formation are poorly studied due to scarcity of outcrops (Lowe and Byerly, 2007).

The Weltevreden Formation rocks as well as the other Onverwacht group units have been subjected to regional metamorphism in the greenschist and locally amphibolite facies. Nonetheless, Weltevreden komatiites are well preserved and contain abundant relicts of fresh olivine grains. The groundmass of the examined samples is completely altered. Here we report the results of studies of three Weltevreden komatiites samples: #1521 (Gary's flow #2), #1522 (Keena's flow #1) and #1523 (Keena's flow #2) that represent the olivine cumulates, collected from the adjacent flows in the Saw Mill area. The detailed description of the sampling site is given in Sobolev et al. (2019).

METHODS

The sample preparation was carried out in the Vernadsky Institute of analytical chemistry and geochemistry, Moscow. The hand specimens were crushed manually or in jaw crusher, sieved to fractions of <0.1 mm, 0.1–0.25 mm, 0.25–0.5 mm, and separated to magnetic and nonmagnetic fractions with a hand magnet. Olivine relicts were collected by handpicking from the non-magnetic fraction of 0.25–0.5 mm size under a binocular microscope.

The most of the melt inclusions were found in central parts of the olivine grains. The melt inclusions typically have a rounded or ellipsoid shape. The maximal dimension of the melt inclusions reaches 250 μm but mostly ranges from 15 to 40 μm. The melt inclusions in the studied samples are partially crystallized and contain residual glass, shrinkage bubble, spinel and clinopyroxene microcrystals and olivine rim along on the inclusion walls (Fig. 2).

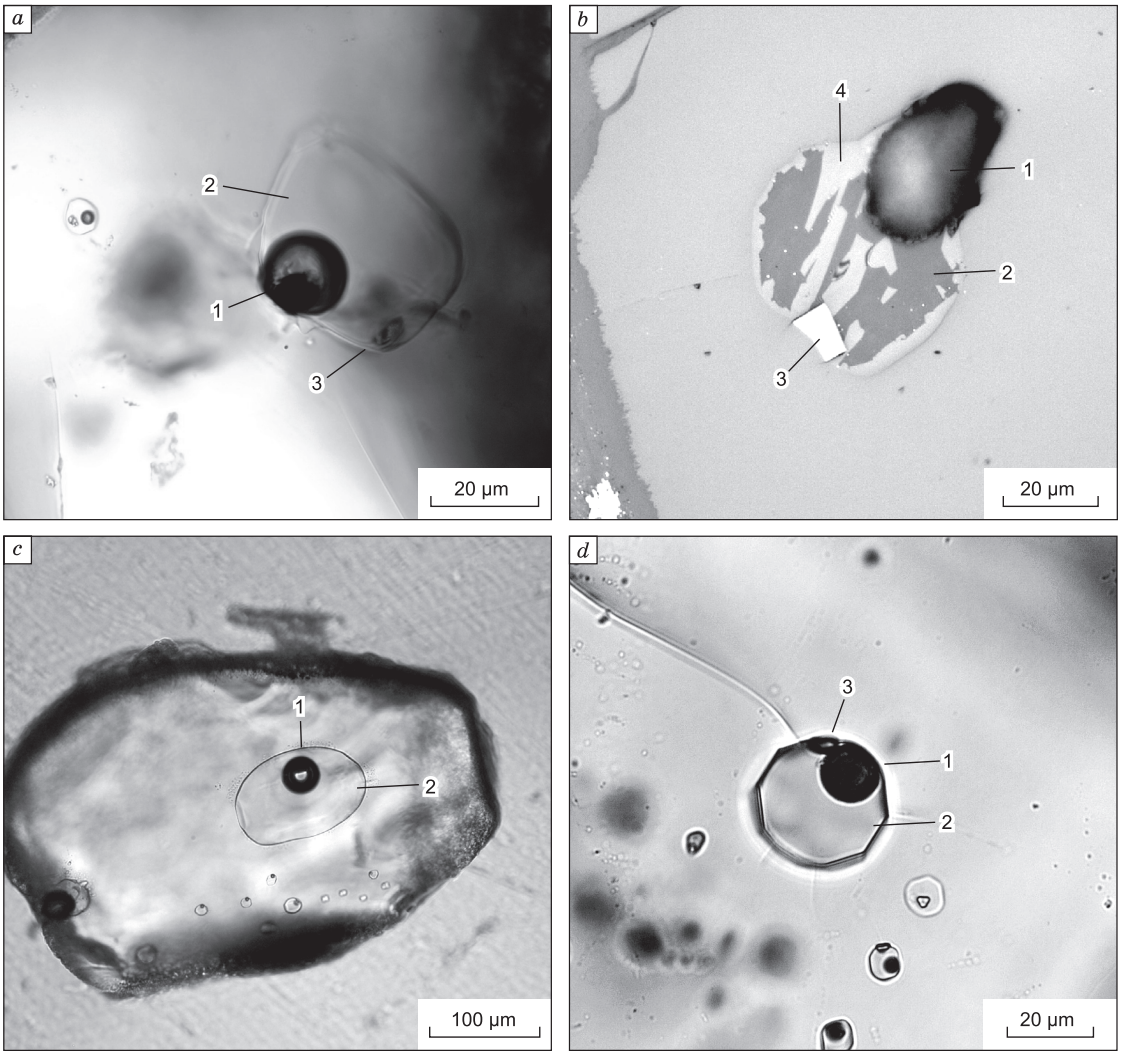

Fig. 2. Olivine hosted melt inclusions from Archean komatiites. *a*, *b*, melt inclusions from Abitibi komatiites, Canada: *a*, heated and quenched (transmitted light); *b*, unheated (thin section, reflected light). *c*, *d*, Quenched melt inclusions from Weltevreden and Belingwe komatiite, respectively (transmitted light). Numbers denote different phases: *1*, shrinkage bubble, *2*, quenched glass, *3*, spinel, *4*, clinopyroxene.

Melt inclusion homogenization. An important part of this study was experimental homogenization of partially crystallized melt inclusions in olivine, which allowed to carry out high precision *in situ* analysis of the inclusions.

To homogenize the melt inclusions, the collected olivine fractions were sealed in platinum capsules and heated in a vertical high temperature furnace Nabertherm RHTV 1700 (Germany), modified for the effective quenching of experimental products (Krasheninnikov et al., 2017). The heating was conducted in a C-O-H atmosphere with controlled oxygen fugacity that corresponded to the quartz-fayalite-magnetite buffer and more reduced conditions (QFM and QFM-1). The first stage of experiments was a 5 min-long pre-heating at 800 °C in the upper section of the furnace in order to flash out all residual air from the capsules. On the second stage, the sample was moved down into the central part of the furnace and heated up to the operational temperature in 5 minutes. The operational temperatures ranged between 1250 to 1520 °C and were individually selected for each sample to achieve the optimal conditions of homogenization depending on the host olivine composition. Quenching was performed by dropping off the capsules in water. After quenching, the melt inclusions were exposed to the surface of olivine grains by grinding and polishing, and prepared for further analyses.

Electron probe microanalysis. Melt inclusions and the host olivine grains were mounted in epoxy and/or indium and analyzed for major and minor element concentrations using the JEOL JXA 8230 electron microprobe in ISTerre, Grenoble, France and applying the method by (Sobolev et al., 2007; Batanova et al., 2015, 2018, 2019). The detailed technique and instrument settings are given in (Sobolev et al., 2016, 2019; Asafov et al., 2018).

LA-ICP-MS. Trace element concentrations in the melt inclusions and their host olivines were analyzed using the quadrupole ICP-MS Agilent 7500s coupled with the 193 nm Excimer laser ablation system GeoLas Pro (Coherent) at the Institute of Geosciences of the Christian-Albrecht University in Kiel, Germany. Details of the analytical technique have been reported elsewhere (Sobolev et al., 2016, 2019; Asafov et al., 2018).

Data processing. Besides the correction for instrumental drift throughout the analytical sessions, the analyzed compositions of melt inclusions were corrected for the effects of *in situ* crystallization of olivine on the walls of inclusions and for Fe–Mg exchange between the trapped melt and host olivine, which results in Fe-loss from melt inclusion. These effects and the ways of their correction are discussed in Danyushevsky et al. (2000).

The reconstruction of the parental melt composition required consideration of both effects that was performed using PETROLOG3 software (Danyushevsky and Plechov, 2011). The olivine-melt models by Ford et al. (1983), and Herzberg and O'Hara (2002) were used in the calculations.

The initial FeO concentrations for each melt inclusion were established depending on the Fo content of the host olivine and calculated by modeling the melt crystallization for each sample series:

1) Crystallization of published primary melt was calculated for the Abitibi komatiites, Canada (Lahaye and Arndt, 1996);

2) For the Belingwe komatiites, Zimbabwe, crystallization of primary melt relevant to Z11 sample was modelled (Bickle et al., 1993). This sample was collected from the chilled margin of the komatiite flow top and represented the parental melt that underwent the least fractional crystallization;

3) For the Barberton komatiites the crystallization of published primary melt was modelled (Kareem, 2005).

RESULTS

The compositions of the Abitibi, Belingwe and Weltevreden melt inclusions and host olivines are described in (Sobolev et al., 2016, 2019; Asafov et al., 2018). It is shown that the komatiite melts were trapped by the most primitive olivines at the earliest stages of magma crystallization. The host olivine compositions range from Fo 92.5 to 90.9 mol.% in Belingwe komatiites, Fo 94.6–92.4 mol.% in Abitibi komatiites and Fo 95.3–93 mol.% in Weltevreden komatiites. For the specified ranges, olivine is the only liquidus phase in the komatiite magma system. Thus, the evolution of komatiite magma compositions within this interval is controlled by olivine fractional crystallization and generally follows so called olivine control line.

The peak equilibrium temperatures of the most MgO-rich olivine-melt pairs in the studied samples that were calculated using model after Ford et al. (1983) and accounted for the lowering effect of the measured water contents on the liquidus temperature (Falloon and Danyushevsky, 2000), are 1450 ºC for Belingwe, 1500 ºC for Abitibi and up to 1520 ºC for Weltevreden (Sobolev et al., 2016, 2019; Asafov et al., 2018).

Belingwe. The measured and corrected melt compositions of the Belingwe komatiites have the lowest MgO contents compared to Abitibi and Weltevreden. The most primitive melt inclusions contain up to 23.6 wt.% MgO. The Al_2O_3/TiO_2 ratio is used to distinguish the geochemical groups of komatiites. In the Belingwe komatiites this ratio is 21, which is comparable to the CI chondrites $Al_2O_3/TiO_2 = 20$ (McDonough and Sun, 1995; Inoue et al., 2000) and corresponds to the Al-undepleted group (Nesbitt et al., 1979).

Abitibi. The melt inclusions from the Abitibi komatiites contain from 22.8 to 28.6 wt.% MgO. The average Al_2O_3/TiO_2 ratio of the Abitibi komatiites is 23 and corresponds to the Al-undepleted group (Nesbitt et al., 1979). This is consistent with the previous reports on the geochemistry of the Pyke Hill and Alexo komatiites (Lahaye and Arndt, 1996; Sproule et al., 2002; Arndt et al., 2008; Sossi et al., 2016).

Weltevreden. The measured and corrected compositions of inclusions in olivine from the Weltevreden komatiites contain 22.1–28.1 wt.% MgO and are characterized by

markedly lower Al_2O_3, CaO и TiO_2 contents and higher SiO_2 compared to Belingwe and Abitibi. Following the classification after Nesbitt et al. (1979) these komatiites fall into the intermediate group between the Al-undepleted and Al-enriched komatiites ($Al_2O_3/TiO_2 > 50$, (Byerly, 1999; Kareem, 2005)).

The major, minor and trace element concentrations in the melt inclusions of all studied samples generally correlate with the MgO contents of the melt and Fo content of the host olivine, and are controlled by the fractional crystallization of olivine (Sobolev et al., 2016, 2019; Asafov et al., 2018). Concentrations of elements, which are immobile at secondary alteration, are consistent with the compositions of whole rocks (Bickle et al., 1993; Lahaye and Arndt, 1996; Sproule et al., 2002; Connolly et al., 2011; Robin-Popieul et al., 2012; Sossi et al., 2016). However, some elements, including Na, K, Rb, Sr, Ba, Cu, Pb, demonstrate enrichment in more evolved melts trapped by less magnesian olivines, which is inconsistent with the fractional crystallization model of magma evolution.

The Abitibi, Belingwe and Weltevreden melts demonstrate significant enrichment in the volatile components such as H_2O (Sobolev et al., 2016, 2019; Asafov et al., 2018) and Cl compared to the modern and primitive mantle (Lyubetskaya and Korenaga, 2007; Kendrick et al., 2017) (Fig. 3). Yet, they have concentrations comparable with those the mantle lithophile element for such elements as Rb (Rb/Nb ratios correspond to those in the Phanerozoic upper mantle, Fig. 3). Cl/K and H_2O/Ce ratios in the examined samples are 0.3–1.1 and 7500 respectively for Abitibi, for Belingwe Cl/K = 1.3–2.5, H_2O/Ce = 1300 and for Weltevreden Cl/K = 2.7–6.3, H_2O/Ce up to 5000, whereas the modern mantle is characterized by Cl/K < 0.2 and H_2O/Ce < 300 (Kendrick et al., 2017).

Cl/K ratios of the Abitibi and Weltevreden melts form strong linear correlations with the Rb/Nb ratios (R^2 = 0.58 and 0.63 respectively, Fig. 3) and with Fo content of the host olivines (Fig. 4). The data on the Phanerozoic ~90 Ma Gorgona komatiites (Echeverria, 1980; Gurenko et al., 2011, 2016) demonstrate comparable to Archean komatiites Cl/K ratios (0.6–1.2) that exceed the typical mantle values and correlate with the forsterite content of the host olivines (Fig. 4). Notably, Cl, K, Rb and Nb are incompatible elements in olivine, and thus the observed correlations cannot result from olivine fractional crystallization. The minimal Cl/K ratios are observed in the most primitive and MgO-rich melt inclusions.

DISCUSSION

Chlorine and water contents in the Earth's mantle. The initial water, chlorine and other volatile element contents of the Earth are uncertain (e.g., Marty, 2012). Yet, the volatile element contents of the Phanerozoic upper mantle were estimated using the compositions of the mid-ocean ridge basalt (MORB) and ocean island basalt (OIB) glasses that possess comparable ratios of H_2O/Ce = 200 ± 100 and Cl/K = 0.06 ± 0.01 (Dixon et al., 2017; Kendrick et al., 2017). As the sources of these basalts are located in different parts of the

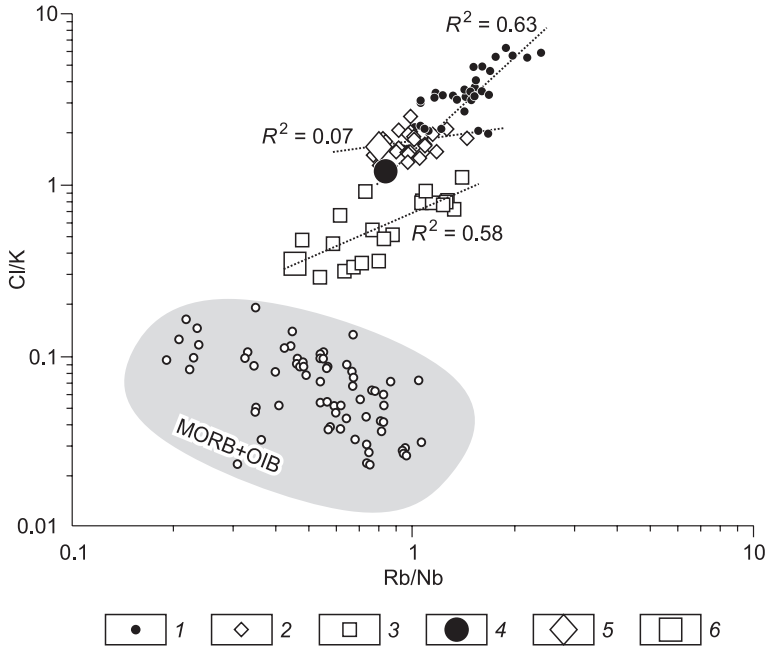

Fig 3. Rb/Nb versus Cl/K in melt inclusions in olivine from Archean komatiites. *1*, Weltevreden; *2*, Belingwe; *3*, Abitibi. Enlarged symbols denote the compositions of initial melts for Weltevreden (*4*), Belingwe (*5*), and Abitibi (*6*), respectively. R^2, squared linear correlation coefficient for different komatiite locations. Mid-ocean ridge basalt (MORB) and ocean island basalt (OIB) glass compositions are shown by small open circles enclosed in grey field (Kendrick et al., 2017).

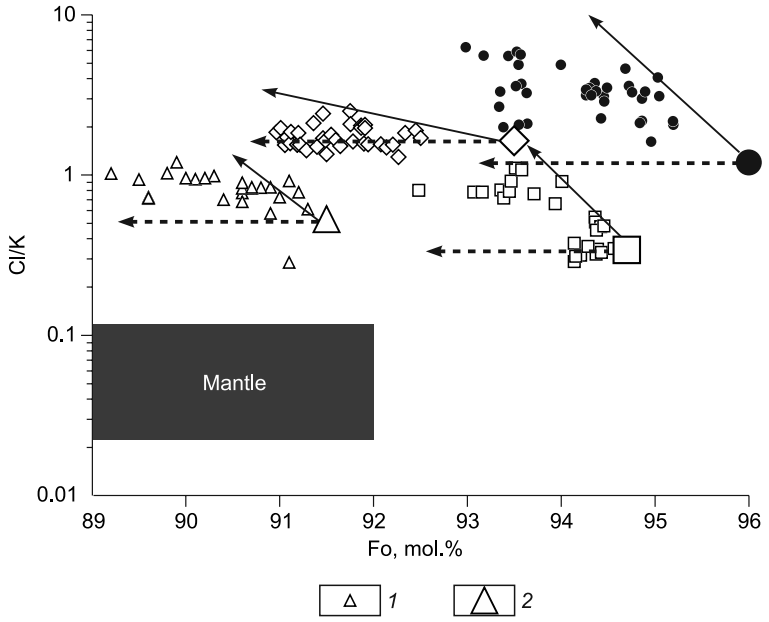

Fig. 4. Variations of Cl/K in melt inclusions from komatiites plotted against Fo content of the host olivine. *1*, Gorgona; *2*, the compositions of initial melts for Gorgona. For other symbols see notation for Fig. 3. Melt inclusion data for Gorgona komatiites are after Gurenko et al. (2011, 2016). Except Belingwe inclusions, Cl/K ratios in the melt inclusions exhibit significant correlations with host olivine composition (Abitibi $R^2 = 0.54$; Weltevreden $R^2 = 0.23$, Gorgona $R^2 = 0.22$). Horizontal dashed arrows represent melt evolution controlled by the olivine fractional crystallization that does not affect Cl/K ratios. Solid arrows denote the trends of assimilation and fractional crystallization (AFC). The composition of typical Phanerozoic mantle is shown by the grey field after (Kendrick et al., 2017).

mantle – in the upper mantle (MORB) and the lower mantle (OIB) (e.g., French and Romanowicz, 2015), the observed ratios are assumed to be typical for the silicate Earth in general. However, the probable exception is the transition mantle zone located at 410–660 km depth, which contains the stable high pressure olivine polymorphs – wadsleyite and ringwoodite. The experimental data suggest (Roberge et al., 2017; Fei and Katsura, 2020) the capability of these phases to concentrate water and chlorine. The direct evidence of high H_2O contents a in ringwoodite inclusion hosted in a diamond confirms the enrichment of the transition zone in water at least beneath the Amazonian craton in the Proterozoic-Phanerozoic times (Pearson et al., 2014). Potentially high Cl content in the deep mantle is suggested by the composition data on diamond hosted inclusions (Izraeli et al., 2001; Logvinova et al., 2008; Sobolev et al., 2009) and unaltered kimberlite melts (Kamenetsky et al., 2004).

The data shown in Figs. 3 and 4 as well as previous results on the H_2O contents in these melt inclusions (Sobolev et al., 2016, 2019; Asafov et al., 2018) show that the studied melts were contaminated by the component enriched in Cl, H_2O, and, in the case of Weltevreden and Abitibi komatiites, in Rb. Furthermore, Abitibi komatiites assimilated LREE enriched component (Sobolev et al., 2016). The probable source of the observed contamination in the Weltevrden and Belingwe komatiites was serpentinite, possibly containing seawater-derived brine. This is confirmed by the element geochemistry and hydrogen isotope composition of the melt inclusions (Asafov et al., 2018; Sobolev et al., 2019). In the case of Abitibi komatiite, the assimilant was likely a serpentinite (Sobolev et al., 2016). These data confirm high chlorine activity in the Archean oceans.

The observed positive correlations between Cl/K and Rb/Nb ratios in the melt inclusions in olivine from the Weltevreden and Abitibi komatiites permit the estimation of the least contaminated or not contaminated melts (Fig. 3). Melt inclusions with the mantle-like Rb/Nb ratios were not or only slightly contaminated and thus can represent the initial komatiite melts for these provinces. The initial Abitibi melt is estimated to have Rb/Nb = 0.45 and Cl/K = 0.34, Weltevreden melt – Rb/Nb = 0.85 and Cl/K = 1.2 (Table 1). The olivine hosted melt inclusions from Belingwe komatiites demonstrate rather constant Cl/K and mantle-like Rb/Nb ratios. Therefore, the initial melt is assumed to have Rb/Nb = 0.8 and Cl/K = 1.64 at the lower limit of the melt inclusions compositions (Table 1).

The calculated H_2O and Cl contents in the initial komatiite magma relative to elements with similar partition coefficient in the melt are shown in Fig. 5 and in Table 1. As komatiites result from high degrees of mantle plume melting (Sobolev et al., 2016, 2019), H_2O/Ce and Cl/K ratios of their initial magmas should represent these ratios in the mantle sources. However, the ratios obtained for komatiites exceed manyfold those of MORB and OIB melts that represent the Phanerozoic Earth's mantle. Since the komatiite magmas are derived from mantle plumes similarly with most OIBs, the anomalous komatiite enrichment in water and chlorine requires an explanation.

Table 1. Major and trace element compositions of melt inclusions in olivine

Component	1523b- o5-i2	1523b-o10	1523b-o13	1523b-o9	1523b-o15	1523b-o12	1523b- o5-i1	1523b-o7	1523b-o11	1523b-ol4	1523b-o6	1523b-o8	1523b-o14	1523b-ol1	1522-ol1
	(30)	(33)	(35)	(38)	(38)	(39)	(44)	(45)	(48)	(54)	(60)	(62)	(65)	(90)	(30.8)
Fo, mol. %	93.34	93.39	93.44	93.55	93.64	93.58	93.35	93.63	93.53	93.57	93.17	93.51	93.55	92.99	94.69
SiO_2, wt. %	50.06	50.67	49.99	49.62	50.12	50.50	49.89	49.64	49.71	49.63	50.07	49.89	49.94	50.08	49.47
TiO_2	0.19	0.187	0.182	0.189	0.198	0.172	0.195	0.189	0.178	0.178	0.188	0.184	0.175	0.195	0.171
Al_2O_3	6.47	6.28	5.93	5.96	6.40	6.25	6.23	6.07	5.98	6.01	6.17	6.04	5.88	6.22	5.65
Fe_2O_3	1.08	1.39	1.07	1.08	1.41	1.43	1.05	1.09	1.07	1.08	1.02	1.13	1.08	0.98	1.64
FeO	9.83	9.55	9.84	9.83	9.43	9.51	9.86	9.72	9.84	9.83	9.98	9.79	9.83	10.12	8.73
MnO	0.13	0.13	0.13	0.13	0.12	0.12	0.12	0.12	0.13	0.12	0.13	0.12	0.12	0.13	0.09
MgO	25.58	25.35	25.87	26.17	25.73	26.03	25.60	26.16	26.19	26.28	25.18	25.97	26.41	24.89	28.58
CaO	5.32	5.42	5.54	5.52	5.58	4.89	5.59	5.52	5.32	5.34	5.67	5.57	5.06	5.63	4.75
Na_2O	0.697	0.651	0.577	0.555	0.646	0.732	0.622	0.618	0.597	0.606	0.622	0.598	0.602	0.625	0.615
K_2O	0.024	0.030	0.028	0.025	0.026	0.034	0.021	0.023	0.035	0.029	0.027	0.023	0.023	0.033	0.023
P_2O_5	0.076	0.019	0.009	0.019	0.008	0.019	0.075	0.013	0.022	0.021	0.013	0.017	0.021	0.017	0.015
Cr_2O_3	0.294	0.338	0.325	0.336	0.326	0.315	0.465	0.344	0.318	0.318	0.344	0.334	0.295	0.342	0.277
Cl	0.053	0.049	0.128	0.101	0.045	0.104	0.058	0.062	0.171	0.136	0.125	0.068	0.039	0.172	0.088
S	0.010	0.006	0.007	0.013	0.017	0.013	0.014	0.009	0.009	0.009	0.011	0.010	0.010	0.013	0.008
Li, ppm	1.98	2.15	2.35	2.02	2.52	1.37	2.01	2.41	2.66	2.09	3.00	2.50	1.89	2.24	1.47
Sc	17.1	15.9	17.3	15.6	20.2	15.5	18.1	18.2	17.1	17.3	21.1	17.0	17.5	19.8	13.4
V	130.0	125.1	138.4	132.7	159.0	98.4	146.3	163.0	164.7	131.6	182.3	147.8	115.1	136.0	108.4
Cu	23.7	32.0	26.2	28.6	33.6	23.7	33.0	39.2	37.7	33.5	42.6	37.3	30.6	39.9	24.4
Rb	0.45	0.57	0.75	0.47	0.45	0.43	0.45	0.53	0.89	0.64	0.64	0.53	0.41	0.79	0.52
Sr	19.5	24.2	26.3	20.2	23.9	20.0	21.3	21.4	26.0	23.4	27.0	22.0	21.7	27.0	20.4
Y	4.04	4.53	4.22	3.73	5.56	4.37	4.37	4.11	3.95	4.01	4.94	4.16	5.06	4.05	4.04
Zr	7.9	7.8	8.7	6.7	9.2	7.1	8.2	7.6	7.3	7.1	8.1	7.6	8.6	8.0	7.4
Nb	0.31	0.34	0.35	0.29	0.37	0.28	0.34	0.37	0.37	0.32	0.36	0.37	0.26	0.42	0.31
Ba	2.9	3.0	3.5	2.4	3.4	2.8	3.1	3.2	3.4	3.2	3.4	3.3	3.1	3.3	2.5
La	0.35	0.36	0.39	0.36	0.41	0.36	0.35	0.39	0.45	0.37	0.42	0.39	0.42	0.38	0.36
Ce	1.37	1.19	1.42	1.19	1.65	1.09	1.31	1.38	1.55	1.25	1.55	1.44	1.47	1.50	1.17
Nd	0.94	0.93	0.84	0.92	1.33	0.96	0.95	0.93	1.14	0.97	1.09	1.07	0.83	1.02	0.96
Sm	0.35	0.39	0.36	0.36	0.50	0.35	0.31	0.37	0.35	0.38	0.45	0.33	0.49	0.32	0.30
Eu	0.15	0.15	0.17	0.16	0.20	0.16	0.16	0.16	0.16	0.15	0.21	0.17	0.17	0.14	0.16
Gd	0.53	0.50	0.52	0.42	0.51	0.46	0.53	0.50	0.38	0.48	0.52	0.50	0.57	0.56	0.59
Dy	0.66	0.75	0.62	0.59	0.81	0.67	0.83	0.67	0.70	0.70	0.89	0.78	0.80	0.75	0.79
Er	0.54	0.50	0.39	0.39	0.60	0.53	0.50	0.53	0.53	0.44	0.50	0.48	0.49	0.47	0.47
Yb	0.50	0.56	0.55	0.41	0.66	0.60	0.60	0.51	0.46	0.50	0.58	0.48	0.62	0.59	0.46
Pb	0.059	0.090	0.120	0.096	0.139	0.103	0.089	0.093	0.125	0.096	0.150	0.093	–	0.178	0.081
Rb/Nb	1.43	1.67	2.18	1.61	1.23	1.53	1.32	1.44	2.39	1.97	1.76	1.43	1.57	1.89	1.70
Cl/K	2.67	1.99	5.52	4.88	2.09	3.70	3.31	3.26	5.87	5.65	5.57	3.57	2.06	6.27	4.62

(*continued on next page*)

Table (*continued*)

Component	1522-ol1p	1522-ol12	1522-ol1	1522-ol3	1522-ol4	1522-ol7	1522-ol5	1522-ol6	1522-ol2	1521-ol9	1521-ol32	1521-ol27	1521-ol13	1521-ol43	1521-ol30
	(31)	(32)	(32)	(34)	(34)	(36)	(59)	(61)	—	(30.4)	(31.2)	(31.5)	(32.6)	(33)	(33.15)
Fo, mol. %	94.36	94.46	94.72	94.00	94.27	94.86	94.30	94.27	94.76	94.49	94.46	95.20	95.28	95.19	94.96
SiO_2, wt. %	49.11	49.18	48.73	49.26	49.72	48.70	49.23	49.18	48.76	49.23	49.71	48.43	48.60	48.77	49.13
TiO_2	0.174	0.172	0.178	0.185	0.184	0.165	0.177	0.19	0.174	0.168	0.165	0.154	0.158	0.169	0.153
Al_2O_3	5.71	5.53	5.74	5.88	5.86	5.59	5.60	5.90	5.74	5.59	5.73	5.20	5.41	5.50	5.47
Fe_2O_3	1.25	1.24	1.36	1.16	1.54	1.36	1.20	1.23	1.40	1.29	1.57	1.45	1.78	1.74	1.71
FeO	9.28	9.19	8.98	9.56	9.02	8.88	9.32	9.30	8.94	9.15	8.89	8.60	8.30	8.34	8.56
MnO	0.09	0.09	0.09	0.11	0.10	0.09	0.10	0.10	0.09	0.09	0.12	0.09	0.09	0.09	0.09
MgO	28.15	28.46	28.97	27.29	27.42	29.50	28.06	27.75	29.13	28.63	28.12	30.66	30.36	29.97	29.63
CaO	4.97	4.82	4.92	5.10	5.19	4.59	4.86	5.13	4.75	4.78	4.88	4.49	4.62	4.73	4.58
Na_2O	0.605	0.586	0.553	0.618	0.618	0.579	0.620	0.595	0.583	0.486	0.432	0.386	0.397	0.402	0.395
K_2O	0.018	0.022	0.019	0.025	0.023	0.019	0.025	0.021	0.027	0.016	0.018	0.018	0.016	0.014	0.019
P_2O_5	0.011	0.015	0.012	0.014	0.247	0.018	0.014	0.015	0.012	0.017	0.013	0.027	0.015	0.007	0.013
Cr_2O_3	0.296	0.267	0.254	0.330	0.091	0.258	0.300	0.289	0.248	0.289	0.350	0.251	0.260	0.270	0.248
Cl	0.056	0.056	0.057	0.101	0.060	0.047	0.072	0.060	0.074	0.047	0.043	0.031	0.064	0.025	0.026
S	0.007	0.013	0.009	0.014	0.008	0.005	0.009	0.012	0.008	0.018	0.004	0.008	0.017	0.016	0.010
Li, ppm	—	1.63	1.63	1.45	1.71	1.49	1.51	1.47	1.99	1.38	—	1.64	—	1.59	1.70
Sc	—	14.7	12.2	13.7	14.6	10.6	12.7	13.6	15.0	15.5	—	13.0	—	13.6	14.1
V	—	107.8	96.9	104.4	137.6	86.4	116.6	117.2	120.5	117.8	—	79.8	—	107.5	83.8
Cu	—	25.9	20.8	22.0	31.8	14.3	26.8	23.8	22.3	29.6	—	16.0	—	21.1	17.5
Rb	—	0.39	0.44	0.53	0.50	0.30	0.45	0.40	0.37	0.46	—	0.29	—	0.30	0.25
Sr	—	16.8	18.9	20.7	23.2	16.0	18.5	19.2	16.3	18.8	—	16.0	—	16.9	17.1
Y	—	3.68	3.84	3.86	4.57	3.47	3.66	4.02	3.33	3.74	—	4.45	—	4.44	4.57
Zr	—	6.4	6.4	7.5	8.4	7.3	7.3	8.0	7.1	6.8	—	7.5	—	7.5	7.9
Nb	—	0.26	0.31	0.35	0.36	0.29	0.31	0.34	0.24	0.29	—	0.26	—	0.30	0.26
Ba	—	2.6	2.7	3.0	3.4	2.4	2.9	2.8	2.2	3.3	—	2.4	—	2.4	2.4
La	—	0.32	0.36	0.41	0.42	0.32	0.34	0.35	0.29	0.35	—	0.30	—	0.35	0.36
Ce	—	1.17	1.14	1.25	1.30	1.13	1.19	1.19	1.03	1.17	—	0.90	—	1.06	0.98
Nd	—	0.84	0.92	0.84	1.00	0.93	0.92	0.97	0.56	0.84	—	0.76	—	0.89	0.86
Sm	—	0.29	0.37	0.41	0.39	0.30	0.37	0.35	0.17	0.25	—	0.26	—	0.35	0.31
Eu	—	0.12	0.14	0.16	0.17	0.10	0.14	0.20	0.09	0.12	—	0.15	—	0.14	0.16
Gd	—	0.46	0.42	0.45	0.62	0.58	0.50	0.48	0.45	0.41	—	0.46	—	0.55	0.55
Dy	—	0.65	0.61	0.65	0.77	0.55	0.65	0.72	0.61	0.56	—	0.82	—	0.68	0.65
Er	—	0.46	0.36	0.56	0.48	0.46	0.43	0.46	0.24	0.39	—	0.46	—	0.51	0.50
Yb	—	0.44	0.33	0.48	0.56	0.42	0.46	0.50	0.28	0.46	—	0.44	—	0.53	0.54
Pb	—	0.097	0.095	0.103	0.093	—	0.089	0.074	0.086		—	0.142	—	0.076	0.084
Rb/Nb	—	1.50	1.43	1.52	1.36	1.06	1.48	1.18	1.52	1.61	—	1.12	—	1.02	0.95
Cl/K	3.75	3.09	3.59	4.87	3.13	3.00	3.49	3.43	3.28	3.51	2.88	2.06	—	2.16	1.62

(*continued on next page*)

Table (*continued*)

Component	1521-ol31	1521-ol2	1521-ol35	1521-ol36	1521-ol30	1521-ol39	1521-ol15	1521-ol78	Weltevreden IM	Abitibi IM	Belingwe IM
	(33.28)	(34.5)	(38)	(39)	(39.7)	(43.4)	(45.2)	—	—	—	—
Fo, mol. %	94.89	94.37	95.05	94.86	95.03	94.84	94.32	94.42	96.00	94.70	93.50
SiO_2, wt. %	49.11	49.28	48.63	48.89	49.12	49.31	49.19	49.45	47.89	45.77	47.00
TiO_2	0.164	0.175	0.157	0.153	0.163	0.167	0.166	0.176	0.140	0.286	0.296
Al_2O_3	5.61	5.64	5.25	5.32	5.54	5.62	5.80	5.87	4.70	6.53	6.44
Fe_2O_3	1.67	1.28	1.41	1.36	1.71	1.65	1.26	1.57	1.13	1.32	0.99
FeO	8.60	9.25	8.73	8.88	8.46	8.61	9.27	8.98	8.23	9.62	10.29
MnO	0.09	0.10	0.09	0.09	0.08	0.09	0.11	0.11	0.08	0.09	0.11
MgO	29.22	28.33	30.27	29.72	29.55	29.08	28.03	28.01	32.9	29.0	27.5
CaO	4.83	4.93	4.55	4.62	4.56	4.72	5.20	5.06	4.06	5.93	6.26
Na_2O	0.407	0.461	0.378	0.418	0.554	0.461	0.422	0.449	0.360	0.534	0.657
K_2O	0.018	0.019	0.017	0.015	0.022	0.018	0.018	0.015	0.014	0.012	0.025
P_2O_5	0.023	0.009	0.015	0.013	0.009	0.018	0.015	0.013	0.01	0.018	0.0169
Cr_2O_3	0.265	0.269	0.249	0.262	0.242	0.257	0.297	0.287	0.240	0.235	0.212
Cl	0.050	0.053	0.044	0.027	0.074	0.032	0.048	0.028	0.014*	0.003*	0.034*
S	0.022	0.019	0.018	0.011	0.005	0.011	0.020	0.015	0.013	0.025	0.024
Li, ppm	1.15	1.28	1.82	1.16	1.28	1.43	1.51	—	1.15	0.56	1.07
Sc	13.4	14.7	12.8	14.6	13.2	15.0	18.6	—	11.9	24.5	19.2
V	91.5	117.7	94.2	97.9	92.3	95.6	107.5	—	82.6	144.2	113.6
Cu	21.8	26.3	20.5	21.7	18.3	20.7	27.7	—	17.4	24.1	42.6
Rb	0.31	0.47	0.28	0.29	0.42	0.28	0.37	—	0.196*	0.127*	0.403*
Sr	17.9	19.1	17.7	17.8	18.3	16.7	20.1	—	15.6	15.5	30.0
Y	4.40	4.07	3.98	4.32	3.77	4.62	5.29	—	3.78	6.93	6.51
Zr	7.7	7.4	7.1	7.8	7.4	8.0	10.1	—	6.6	12.4	12.8
Nb	0.25	0.28	0.26	0.27	0.28	0.25	0.32	—	0.23	0.28	0.50
Ba	2.2	2.8	2.3	2.3	2.5	2.4	2.7	—	2.2	2.3	5.4
La	0.34	0.32	0.38	0.36	0.34	0.32	0.44	—	0.30	0.29	0.62
Ce	0.96	1.15	1.15	0.97	1.13	0.99	1.15	—	0.91	0.93	1.74
Nd	0.90	0.81	0.99	0.87	0.85	0.92	1.11	—	0.77	1.14	1.67
Sm	0.34	0.39	0.34	0.27	0.27	0.40	0.40	—	0.28	0.52	0.62
Eu	0.14	0.14	0.15	0.12	0.11	0.14	0.15	—	0.12	0.21	0.25
Gd	0.56	0.44	0.55	0.52	0.49	0.54	0.62	—	0.45	0.84	0.92
Dy	0.69	0.72	0.71	0.67	0.59	0.78	0.88	—	0.62	1.22	1.16
Er	0.50	0.45	0.50	0.52	0.43	0.51	0.63	—	0.43	0.71	0.74
Yb	0.53	0.48	0.44	0.51	0.38	0.52	0.67	—	0.43	0.77	0.69
Pb	0.071	0.056	0.061	0.127	0.065	0.057	0.069	—	0.057	0.056	0.108
Rb/Nb	1.23	1.68	1.06	1.06	1.54	1.09	1.17	—	0.85*	0.45*	0.8*
Cl/K	3.32	3.34	3.10	2.17	4.06	2.12	3.19	2.26	1.2*	0.34*	1.64*

Note. Compositions of melt inclusions and the initial melt (IM) for Weltevreden komatiites are from this study. Initial melt compositions for Belingwe and Abitibi komatiites are after Asafov et al. (2018) and Sobolev et al. (2016). Samples of Weltevreden komatiites (##1523, 1522 and 1521) represent cumulate layers of three adjacent flows (see text and supplementary material in (Sobolev et al., 2019)).

*The initial melt ratios were determined using the correlation between Rb/Nb and Cl/K for the least contaminated melt inclusions (see text for details).

In a series of earlier papers (Sobolev et al., 2016, 2019; Asafov et al., 2018), we suggested that the excessive H_2O contents in komatiite initial melts could be related to the interaction with the transition mantle zone enriched in water (Pearson et al., 2014). In contrast to the common Phanerozoic mantle plumes, komatiites have high potential temperatures over 1650 °C (Robin-Popieul et al., 2012; Sobolev et al., 2019), which are sufficiently high for the partial melting throughout the transition mantle zone (Andrault et al., 2018). The melt forms an interstitial network within the ascending Archean mantle plume and therefore effectively transports water molecules from the enriched transition zone into the plume, which is not the case for the less hot and solid Phanerozoic mantle plumes. One exception is the Phanerozoic Caribbean mantle plume (Trela et al., 2017) that reached temperatures characteristic of the Archean plumes and thus traversed the mantle transition zone in a partially molten state and generated the Gorgona komatiites.

The chlorine excess in the komatiite mantle sources can be explained by the same mechanism as for the water excess, namely draining of this component from the mantle transition zone. In fact, the major mantle phases ringwoodite and wadsleyite can contain high chlorine concentrations as was demonstrated experimentally (Roberge et al., 2017). Moreover, the microinclusions of Cl-bearing carbonatites in diamonds suggest the high activity of the chlorine component in mantle (Izraeli et al., 2001; Logvinova et al., 2008; Sobolev et al., 2009).

The source of chlorine and water in the Earth's mantle. Chlorine and water are the major components of the seawater since at least 3.3 Ga. This is evidenced by the data on the Weltevreden komatiites contaminated by chlorine and water enriched material (Fig. 3) (this study; Sobolev et al. 2019). The seafloor alteration via the reaction of oceanic crust with the seawater results in formation of the low temperature enriched in H_2O and Cl minerals of the serpentine and chlorite group, e.g., Kodolányi et al. (2011). Several researchers point out that the seawater derived alteration may affect the contemporary oceanic lithosphere to the depths of 10 km and even deeper (e.g., Michael and Schilling 1989; Bazylev, 1992; Michael and Cornell, 1998). Subduction of the altered oceanic lithosphere results in the loss of most water and a significant fraction of chlorine into the mantle wedge and subsequently into the suprasubduction magmas. However, a substantial amount of these components is transported into the deep mantle in the subducting slab down to the mantle plume sources (Stroncik and Haase, 2004; Hanyu et al., 2019; Page and Hattori, 2019). Therefore, it is plausible that the excessive chlorine and water contents in the mantle transition zone and in the komatiite plume source originates from the seawater altered oceanic lithosphere descended into the deep mantle (Figs. 5, 6).

Implications for the Archean geodynamics on Earth. An important result of this study and Sobolev et al. (2019) is the evidence for the transport of seawater reworked material into the deep mantle that began >3.3 Ga. So far such evidence was provided only for the period of 2.5 Ga (Hanyu et al., 2019). This result contributes to the understanding of the Earth's geodynamics during the first billion years of the planet history.

Most researchers agree that the onset of the global plate tectonics, which controls modern geodynamics of Earth, took place at the turn of the Archean and Proterozoic eons or later (Hawkesworth et al., 2017). Many researchers assume that prior to plate tectonics, the stagnant lid regime operated and involved descending lower crust fragments into the deep mantle via delamination (e.g., review by Hawkesworth et al. (2017)). To delaminate the upper crust reworked by seawater, the crust needs to sink down to the boundary with the lithospheric mantle and be eclogitized under low pressures and high temperatures, i.e. under conditions of high temperature gradient (Sizova et al., 2015; Gerya, 2019). However, such a process would cause almost complete degassing of the seawater derived volatile components from the descending crust (Roman and Arndt, 2020) and thus is inappropriate for explanation of the results obtained in this study. The partial retaining of water and chlorine in the altered crust is possible under subduction regime occurring at low thermal gradient. Under these conditions, serpentinites can keep and transport up to 15% Cl and 5% H_2O of the

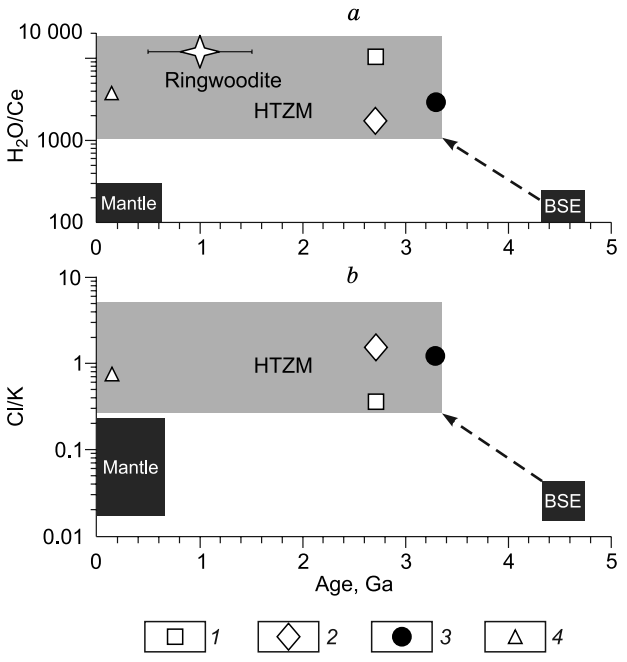

Fig. 5. The temporal evolution of H_2O/Ce (*a*) and Cl/K (*b*) in the initial komatiite melts and Earth's mantle reservoirs. Figure *a* was modified after Sobolev et al. (2019). Initial komatiite melts: *1*, Abitibi; *2*, Belingwe; *3*, Weltevreden; *4*, Gorgona. Ringwoodite composition shows the diamond hosted inclusion after Pearson et al. (2014). Melt inclusion data for Gorgona komatiites are after Gurenko et al. (2011, 2016). The compositions of the bulk silicate Earth (BSE, black field) (Hofmann, 1988), hydrated transition zone of the mantle (HTZM, grey field) (Sobolev et al., 2019), and Phanerozoic mantle (black field) (Kendrick et al., 2017) are shown for reference.

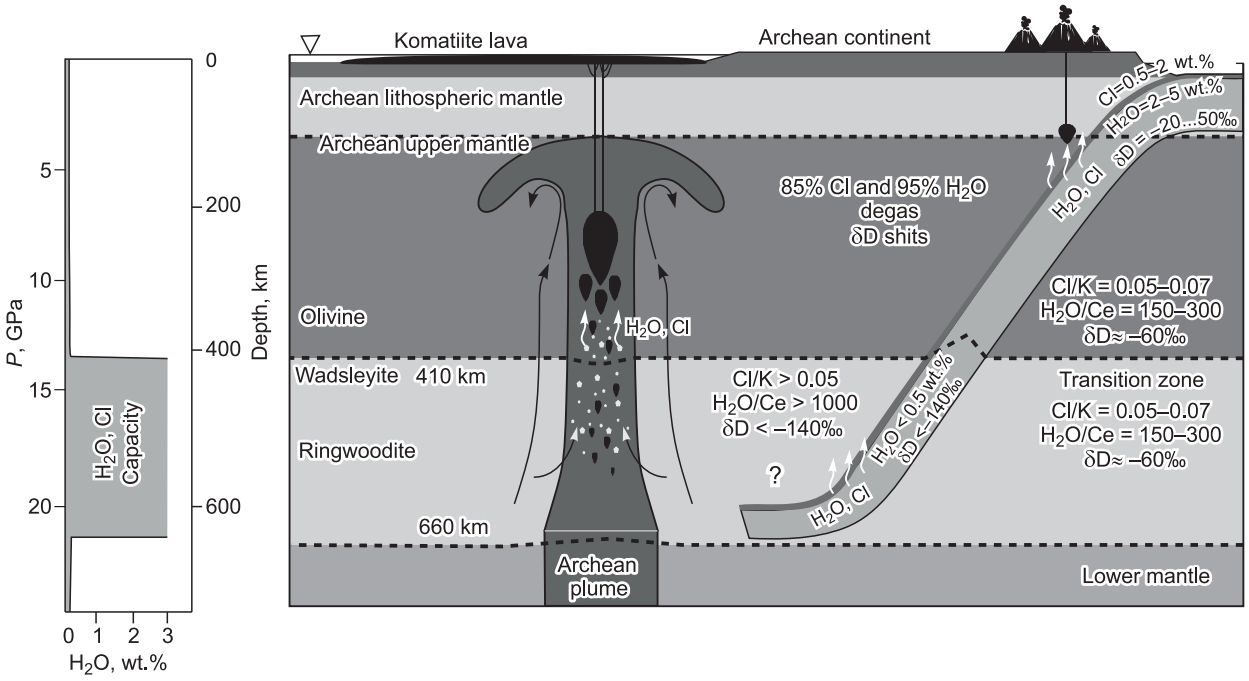

Fig. 6. The model of mantle plume enrichment by recycled chlorine and water. Partially molten Archean plume traverses the mantle transition zone and captures its material. This material contains high pressure olivine polymorphs enriched in chlorine and water (Inoue, 2000; Bercovici and Karato, 2003; Roberge et al., 2017). Water and chlorine are supplied into the transition zone with the subducted oceanic lithosphere altered by seawater. As the mantle plume ascends, the olivine is transformed into the low pressure polymorph and loses Cl and H_2O. The release of aqueous component from solid phases lowers the solidus temperature of the mantle peridotite that leads to the intensive partial melting and generation of komatiite magma.

initial concentrations after the shallow dehydration into the deep mantle (Shaw et al., 2008; Page and Hattori, 2019). Stagnation of the subducted plates in the transition mantle zone for hundreds million years could result in the significant enrichment of this zone with chlorine and water and in formation of the geochemical reservoir sourcing komatiites (Fig. 6).

Our results suggest that the subduction-like process had operated for several hundred million years before 3.3 Ga, when the chlorine- and water-rich mantle source had emerged in the Weltevreden komatiite initial magmas. This regime was not necessarily identical to the modern plate tectonics. It could be the regime of "minor plate tectonics" (Dobretsov and Turkina, 2015) involving the mechanism of retreating subduction zones (Sobolev and Brown, 2019). Either way, our data demonstrate that seawater altered material should have been able to descend to more than 400 km depth in the first billion years of the Earth's history.

CONCLUDING REMARKS

We report new data on the compositions of the homogenized melt inclusions and host olivines from the Archean komatiites of 3.3 Ga Barberton Greenstone Belt, Weltevreden Formation, South Africa; 2.72 Ga Abitibi Greenstone Belt, Canada; and 2.69 Ga Belingwe Greenstone Belt, Zimbabwe.

Olivine crystallization in the komatiite melts was accompanied by the assimilation of Rb, Cl and H_2O enriched crustal material.

Uncontaminated komatiite melts possess the mantle-like Rb/Nb ratios, but exhibit large enrichment in Cl and H_2O relative to similarly incompatible elements, K and Ce, respectively.

The enrichment in Cl and H_2O of the komatiite mantle sources were observed in the Earth's history since 3.3 Ga and until at least 90 Ma.

The excessive Cl and H_2O concentrations in the komatiite sources were supplied into the hot and partially molten mantle plumes traversing the mantle transition zone.

The enrichment in Cl and H_2O of the Earth's deep mantle originated from the seawater altered oceanic lithosphere.

The descending of altered oceanic lithosphere into the deep mantle started in the first billion years of Earth's history via subduction process. Crustal delamination cannot explain the transport of chlorine and water into the deep mantle.

ACKNOWLEDGMENTS

We thank S. Krasheninnikov for help with the high temperature experiments, V. Turkov for help with sample preparation, Dieter Garbe-Schönberg and Ulrike Westernstroer for assistance with LA-ICP-MS analyses, N. Arndt, G. Byerly, and A. Wilson for help during field work in Canada and

South Africa. The field work was funded by the Russian Science Foundation grant № 14-17-00491 (to A. Sobolev). The work in Vernadsky Institute of Geochemistry and Analytical Chemistry was supported by the state assignment funds on the topic "Petrology, geochemistry and geodynamics of the oceanic and continental lithosphere formation processes and evolution". The experimental laboratory in Vernadsky Institute of Geochemistry and Analytical Chemistry was maintained by funds of the Russian Foundation of Basic Research grant № 17-05-00856. The analytical facility in ISTerre was supported by the Academic Institute of France (Institut universitaire de France, IUF). The authors thank two anonymous reviewers for their precious comments on the initial version of the paper.

REFERENCES

Andrault, D., Pesce, G., Manthilake, G., Monteux, J., Bolfan-Casanova, N., Chantel, J., Novella, D., Guignot, N., King, A., Itié, J.-P., Hennet, L., 2018. Deep and persistent melt layer in the Archaean mantle. Nat. Geosci. 11 (2), 139–143.

Armstrong, R.A., Compston, W., De Wit, M.J., Williams, I.S., 1990. The stratigraphy of the 3.5–3.2 Ga Barberton Greenstone Belt revisited: A single zircon ion microprobe study. Earth Planet. Sci. Lett. 101 (1), 90–106.

Arndt, N.T.., Naldrett, A.J., Pyke, D.R., 1977. Komatiitic and iron-rich tholeiitic lavas of Munro Township, northeast Ontario. J. Petrol. 18 (2), 319–369.

Arndt, N.T., Lesher, C.M., Barnes, S.J., 2008. Komatiite. Cambridge university press, New York.

Asafov, E.V., Sobolev, A.V., Gurenko, A.A., Arndt, N.T., Batanova, V.G., Portnyagin, M.V., Garbe-Schönberg, D., Krasheninnikov S.P., 2008. Belingwe komatiites (2.7 Ga) originate from a plume with moderate water content, as inerred from inclusions in olivine. Chem. Geol. 478, 39–59.

Batanova, V.G., Sobolev, A.V., Magnin, V., 2008. Trace element analysis by EPMA in geosciences: detection limit, precision and accuracy. IOP Conf. Ser.: Mater. Sci. Eng. 304, Article 012001.

Batanova, V.G., Sobolev, A.V., Kuzmin, D.V., 2015. Trace element analysis of olivine: High precision analytical method for JEOL JXA-8230 electron probe microanalyser. Chem. Geol. 419, 149–157.

Batanova, V.G., Thompson, J.M., Danyushevsky, L.V., Portnyagin, M.V., Garbe-Schönberg, D., Hauri, E., Kimura, J.I., Chang, Q., Senda, R., Goemann, K., Chauvel, C., Campillo, S., Ionov, D., Sobolev, A.V., 2019. New olivine reference material for *in situ* microanalysis. Geostand. Geoanal. Res. 43 (3), 453–473.

Bazylev, B.A., 1992. Metamorphism of peridotites from the Atlantis fault zone (Atlantic Ocean) – an evidence of deep penetration of water into oceanic lithosphere. Dokl. Akad. Nauk 323 (4), 741–743.

Bercovici, D., Karato, S., 2003. Whole-mantle convection and the transition-zone water filter. Nature 425 (6953), 39–44.

Bickle, M.J., Martin, A., Nisbet, E.G., 1975. Basaltic and peridotitic komatiites and stromatolites above a basal unconformity in Belingwe Greenstone Belt, Rhodesia. Earth Planet. Sci. Lett. 27 (2), 155–162.

Bickle, M.J., Ford, C.E., Nisbet, E.G., 1977. Petrogenesis of peridotitic komatiites – evidence from high-pressure melting experiments. Earth Planet. Sci. Lett. 37 (1), 97–106.

Bickle, M.J., Arndt, N.T., Nisbet, E.G., Orpen, J.L., Martin, A., Keays, R.R., Renner, R. 1993. Geochemistry of the igneous rocks of the Belingwe greenstone belt: alteration, contamination and petrogenesis, in: Bickle, M.J., Nisbet, E.G., Orpen, J.L. (Eds.), 1993.The Geology of the Belingwe Greenstone Belt, Zimbabwe: a Study of Archaean Continental Crust. CRC Press, Boca Raton, London, New York, pp. 175–213.

Brévart, O., Dupré, B., Allègre, C.J., 1986. Lead-lead age of komatiitic lavas and limitations on the structure and evolution of the Precambrian mantle. Earth Planet. Sci. Lett. 77 (3–4), 293–302.

Byerly, G.R., 1999. Komatiites of the Mendon Formation: late-stage ultramafic volcanism in the Barberton Greenstone Belt, in: Lowe, D.R., Byerly, G.R. (Eds.), Geological Evolution of the Barberton Greenstone Belt. Spec. Pap. Geol. Soc. Am., pp. 189–212.

Byerly, G.R., Kröner, A., Lowe, D.R., Todt, W., Walsh, M.M., 1996. Prolonged magmatism and time constraints for sediment deposition in the early Archean Barberton greenstone belt: evidence from the Upper Onverwacht and Fig Tree groups. Precambrian Res. 78 (1–3), 125–138.

Connolly, B.D., Puchtel, I.S., Walker, R.J., Arevalo Jr., R., Piccoli, P.M., Byerly, G., Robin-Popieul, C., Arndt, N., 2011. Highly siderophile element systematics of the 3.3 Ga Weltevreden komatiites, South Africa: implications for early Earth history. Earth Planet. Sci. Lett. 311 (3–4), 253–263.

Danyushevsky, L.V., Plechov, P., 2011. Petrolog3: Integrated software for modeling crystallization processes. Geochem. Geoph. Geosyst. 12, Article Q07021, doi: 10.1029/2011GC003516.

Danyushevsky, L.V., Della-Pasqua, F.N., Sokolov, S., 2000. Re-equilibration of melt inclusions trapped by magnesian olivine phenocrysts from subduction-related magmas: petrological implications. Contrib. Mineral. Petrol. 138 (1), 68–83.

Dixon, J.E., Bindeman, I.N., Kingsley, R.H., Simons, K.K., Le Roux, P.J., Hajewski, T.R., Swart, P., Langmuir, C.H., Ryan, J.G., Walowski, K.J., Wada, I., 2017. Light stable isotopic compositions of enriched mantle sources: Resolving the dehydration paradox. Geochem. Geophys. Geosyst. 18 (11), 3801–3839.

Dobretsov, N.L., Turkina, O.M., 2015. Early Precambrian Earth history: Plate and plume tectonics and extraterrestrial controls. Russian Geology and Geophysics (Geologiya i Geofizika) 56 (7), 978–995 (1250–1274).

Dupre, B., Arndt, N.T., 1990. Pb isotopic compositions of Archean komatiites and sulfides. Chem. Geol. 85 (1–2), 35–56.

Echeverria, L.M., 1980. Tertiary or Mesozoic komatiites from Gorgona Island, Colombia: Field relations and geochemistry. Contrib. Mineral. Petrol. 73 (3), 253–266.

Falloon, T.J., Danyushevsky, L.V., 2000. Melting of refractory mantle at 1.5, 2 and 2.5 GPa under anhydrous and H_2O-undersaturated conditions: Implications for the petrogenesis of high-Ca boninites and the influence of subduction components on mantle melting. J. Petrol. 41 (2), 257–283.

Fei, H., Katsura, T., 2020. High water solubility of ringwoodite at mantle transition zone temperature. Earth Planet. Sci. Lett. 531, Article 115987.

Ford, C.E., Russell, D.G., Craven, J.A., Fisk, M.R., 1983. Olivine liquid equilibria: temperature, pressure and composition dependence of the crystal liquid cation partition coefficients for Mg, Fe-2+, Ca and Mn. J. Petrol. 24 (3), 256–266.

French, S.W., Romanowicz, B., 2015. Broad plumes rooted at the base of the Earth's mantle beneath major hotspots. Nature 525 (7567), 95–99.

Gerya, T., 2019. Introduction to numerical geodynamic modelling. Cambridge University Press, Cambridge.

Gurenko, A.A., Kamenetsky, V.S., 2011. Boron isotopic composition of olivine-hosted melt inclusions from Gorgona komatiites, Colombia: New evidence supporting wet komatiite origin. Earth Planet. Sci. Lett. 312 (1–2), 201–212.

Gurenko, A.A., Kamenetsky, V.S., Kerr, A.C., 2016. Oxygen isotopes and volatile contents of the Gorgona komatiites, Colombia: A confirmation of the deep mantle origin of H_2O. Earth Planet. Sci. Lett. 454, 154–165.

Hanyu, T., Shimizu, K., Ushikubo, T., Kimura, J.I., Chang, Q., Hamada, M., Ito, M., Iwamori, H., Ishikawa, T., 2019. Tiny droplets of ocean island basalts unveil Earth's deep chlorine cycle. Nat. Commun. 10 (1), Article 60.

Hawkesworth, C.J., Cawood, P.A., Dhuime, B., Kemp, T.I.S., 2017. Earth's continental lithosphere through time. Ann. Rev. Earth Planet. Sci. 45, 169–198.

Herzberg, C., 2016. Petrological evidence from komatiites for an early Earth carbon and water cycle. J. Petrol. 57 (11–12), 2271–2288.

Herzberg, C., O'Hara, M.J., 2002. Plume-associated ultramafic magmas of phanerozoic age. J. Petrol. 43 (10), 1857–1883.

Hofmann, A.W., 1988. Chemical differentiation of the Earth: The relationship between mantle, continental crust, and oceanic crust. Earth Planet. Sci. Lett. 90 (3), 297–314.

Inoue, T., Rapp, R.P., Zhang, J., Gasparik, T., Weidner, D.J., Irifune, T., 2000. Garnet fractionation in a hydrous magma ocean and the origin of Al-depleted komatiites: melting experiments of hydrous pyrolite with REEs at high pressure. Earth Planet. Sci. Lett. 177 (1–2), 81–87.

Izraeli, E.S., Harris, J.W., Navon, O., 2001. Brine inclusions in diamonds: a new upper mantle fluid. Earth Planet. Sci. Lett. 187 (3–4), 323–332.

Kamenetsky, M.B., Sobolev, A.V., Kamenetsky, V.S., Maas, R., Danyushevsky, L.V., Thomas, R., Pokhilenko, N.P., Sobolev, N.V., 2004. Kimberlite melts rich in alkali chlorides and carbonates: A potent metasomatic agent in the mantle. Geology 32 (10), 845–848.

Kamenetsky, V.S., Gurenko, A.A., Kerr, A.C., 2010. Composition and temperature of komatiite melts from Gorgona Island, Colombia, constrained from olivine-hosted melt inclusions. Geology 38 (11), 1003–1006.

Kareem, K., 2005. Komatiites of the Weltevreden Formation, Barberton Greenstone Belt, South Africa: implications for the chemistry and temperature of the Archean mantle. LSU Doctoral Dissertation, 3249.

Kendrick, M.A., Hémond, C., Kamenetsky, V.S., Danyushevsky, L., Devey, C.W., Rodemann, T., Jackson, M.G., Perfit, M.R., 2017. Seawater cycled throughout Earth's mantle in partially serpentinized lithosphere. Nat. Geosci. 10 (3), 222–228.

Kodolányi, J., Pettke, T., Spandler, C., Kamber, B.S., Gméling, K., 2011. Geochemistry of ocean floor and fore-arc serpentinites: constraints on the ultramafic input to subduction zones. J. Petrol. 53 (2), 235–270.

Korenaga, J., 2008. Urey ratio and the structure and evolution of Earth's mantle. Rev. Geophys. 46 (2), Article 2007RG000241.

Krasheninnikov, S.P, Sobolev, A.V, Batanova, V.G, Kargaltsev, A.A, Borisov, A.A., 2017. Experimental testing of olivine–melt equilibrium models at high temperatures. Dokl. Earth Sci. 475 (2), 919–922.

Kröner, A., Hegner, E., Wendt, J., Byerly, G., 1996. The oldest part of the Barberton granitoid-greenstone terrain, South Africa: evidence for crust formation between 3.5 and 3.7 Ga. Precambrian Res. 78 (1–3), 105–124.

Lahaye, Y., Arndt, N., 1996. Alteration of a komatiite flow from Alexo, Ontario, Canada. J. Petrol. 37 (6), 1261–1284.

Logvinova, A.M., Wirth, R., Fedorova, E.N., Sobolev, N.V., 2008. Nanometre-sized mineral and fluid inclusions in cloudy Siberian diamonds: New insights on diamond formation. Eur. J. Mineral. 20 (3), 317–331.

Lowe, D.R., Byerly, G.R., 2007. An Overview of the Geology of the Barberton Greenstone belt and Vicinity: Implications for Early Crustal Development. Dev. Precambrian Geol. 15, 481–526.

Lyubetskaya, T., Korenaga, J., 2007. Chemical composition of Earth's primitive mantle and its variance: 1. Method and results. J. Geophys. Res: Solid Earth 112 (B3), Article B03211.

Marty, B., 2012. The origins and concentrations of water, carbon, nitrogen and noble gases. Earth Planet. Sci. Lett. 313, 56–66.

McDonough, W.F., Sun, S.-S., 1995. The composition of the Earth. Chem. Geol. 120 (3–4), 223–253.

Michael, P.J., Schilling, J.G., 1989. Chlorine in mid-ocean ridge magmas: evidence for assimilation of seawater-influenced components. Geochim. Cosmochim. Acta 53 (12), 3131–3143.

Michael, P.J., Cornell, W.C., 1998. Influence of spreading rate and magma supply on crystallization and assimilation beneath mid-ocean ridges: Evidence from chlorine and major element chemistry of mid-ocean ridge basalts. J. Geoph. Res.: Solid Earth 103 (B8), 18325–18356.

Muir, J., Comba, C., 1979. The Dundonald deposit; an example of volcanic-type nickel-sulfide mineralization. Can. Mineral. 17 (2), 351–359.

Nesbitt, R., Sun, S.-S., Purvis, A., 1979. Komatiites; geochemistry and genesis. Can. Mineral. 17 (2), 165–186.

Nisbet, E.G., Bickle, M.J., Martin, A., 1977. Mafic and ultramafic lavas of Belingwe Greenstone Belt, Rhodesia. J. Petrol. 18 (4), 521–566.

Pagé, L., Hattori, K., 2019. Abyssal serpentinites: transporting halogens from Earth's surface to the deep mantle. Minerals 9 (1), Article 61.

Pearson, D.G., Brenker, F.E., Nestola, F., McNeill, J., Nasdala, L., Hutchison, M.T., Matveev, S., Mather, K., Silversmit, G., Schmitz, S., Vekemans, B., 2014. Hydrous mantle transition zone indicated by ringwoodite included within diamond. Nature 507 (7491), 221–224.

Pyke, D., Naldrett, A., Eckstrand, O., 1973. Archean ultramafic flows in Munro township, Ontario. Geol. Soc. Am. Bull. 84 (3), 955–978.

Roberge, M., Bureau, H., Bolfan-Casanova, N., Raepsaet, C., Surble, S., Khodja, H., Auzende, A.L., Cordier, P., Fiquet, G., 2017. Chlorine in wadsleyite and ringwoodite: An experimental study. Earth Planet. Sci. Lett., 467, 99–107.

Robin-Popieul C., Arndt N.T., Chauvel C., Byerly G., Sobolev A.V., Wilson A., 2012. A new model for Barberton Komatiites: deep critical melting with high melt retention. J. Petrol. 53 (11), 2191–2229.

Roman, A., Arndt, N., 2020. Differentiated Archean oceanic crust: Its thermal structure, mechanical stability and a test of the sagduction hypothesis. Geochim. Cosmochim. Acta, 278, 65–77.

Shaw, A., Hauri, E., Fischer, T., Hilton, D., Kelley, K., 2008. Hydrogen isotopes in Mariana arc melt inclusions: Implications for subduction dehydration and the deep-Earth water cycle. Earth Planet. Sci. Lett. 275 (1–2), 138–145.

Sizova, E., Gerya, T., Stüwe, K., Brown, M., 2015. Generation of felsic crust in the Archean: a geodynamic modeling perspective. Precambrian Res. 271, 198–224.

Sobolev, A.V., Hofmann, A.W., Kuzmin, D.V., Yaxley, G.M., Arndt, N.T., Chung, S.L., Danyushevsky, L.V., Elliott, T., Frey, F.A., Garcia, M.O., Gurenko, A.A., Kamenetsky, V.S., Kerr, A.C., Krivolutskaya, N.A., Matvienkov, V.V., Nikogosian, I.K., Rocholl, A., Sigurdsson, I.A., Sushchevskaya, N.M., Teklay, M., 2007. The amount of recycled crust in sources of mantle-derived melts. Science 316 (5823), 412–417.

Sobolev, A.V., 1996. Melt inclusions in minerals as a source of principle petrological information. Petrology 4 (3), 209–220.

Sobolev, A.V., Asafov, E.V., Gurenko, A.A., Arndt, N.T., Batanova, V.G., Portnyagin, M.V., Garbe-Schönberg, D., Krasheninnikov, S.P., 2016. Komatiites reveal a hydrous Archaean deep-mantle reservoir. Nature 531 (7596), 628–632.

Sobolev, A.V., Asafov, E.V., Gurenko, A.A., Arndt, N.T., Batanova, V.G., Portnyagin, M.V., Garbe-Schönberg, D., Wilson, A.H., Byerly, G.R. 2019. Deep hydrous mantle reservoir provides evidence for crustal recycling before 3.3 billion years ago. Nature 571 (7766), 555–559.

Sobolev, N.V., Logvinova, A.M., Efimova, E.S., 2009. Syngenetic phlogopite inclusions in kimberlite-hosted diamonds: implications for role of volatiles in diamond formation. Russian Geology and Geophysics (Geologiya i Geofizika) 50 (12), 1234–1248 (1588–1606).

Sobolev, S.V., Brown, M., 2019. Surface erosion events controlled the evolution of plate tectonics on Earth. Nature 570 (7759), 52–57.

Sossi, P.A., Eggins, S.M., Nesbitt, R.W., Nebel, O., Hergt, J.M., Campbell, I.H., O'Neill, H.S.C., Van Kranendonk, M., Davies, D.R., 2016. Petrogenesis and geochemistry of Archean komatiites. J. Petrol. 57 (1), 147–184.

Sproule, R., Lesher, C., Ayer, J., Thurston, P., Herzberg, C., 2002. Spatial and temporal variations in the geochemistry of komatiites and komatiitic basalts in the Abitibi greenstone belt. Precambrian Res. 115 (1), 153–186.

Stroncik, N.A., Haase, K.M., 2004. Chlorine in oceanic intraplate basalts: Constraints on mantle sources and recycling processes. Geology 32 (11), 945–948.

Trela, J., Gazel, E., Sobolev, A.V., Moore, L., Bizimis, M., Jicha, B., Batanova, V.G., 2017. The hottest lavas of the Phanerozoic and the survival of deep Archaean reservoirs. Nat. Geosci. 10 (6), 451–456.

Editorial responsibility: N.V. Sobolev